J Therm Anal Calorim (2011) 106:507–512
DOI 10.1007/s10973-011-1509-6

Crystallization study of $SrSnO_3$:Fe

F. T. G. Vieira · A. L. M. Oliveira · D. S. Melo · S. J. G. Lima · E. Longo · A. S. Maia · A. G. Souza · I. M. G. Santos

CBRATEC7 Conference Special Issue

Abstract Alkaline earth stannates have recently become important materials in ceramic technology due to its application as humidity sensor. In this work, alkaline earth stannates doped with Fe^{3+} were synthesized by the polymeric precursor method, with calcination at 300 °C/7 h and between 400 and 1100 °C/4 h. The powder precursors were characterized by TG/DTA after partial elimination of carbon. Characterization after the second calcination step was done by X-ray diffraction, infrared spectroscopy, and UV–vis spectroscopy. Results confirmed the formation of the $SrSnO_3$:Fe with orthorhombic perovskite structure, besides $SrCO_3$ as secondary phase. Crystallization occurred at 600 °C, being much lower than the crystallization temperature of perovskites synthesized by solid state reaction. The analysis of TG curves indicated that the phase crystallization was preceded by two thermal decomposition steps. Carbonate elimination occurred at two different temperatures, around 800 °C and above 1000 °C.

Keywords TG/DTA · Fe^{3+} · Crystallization

F. T. G. Vieira · A. L. M. Oliveira · D. S. Melo · A. S. Maia · A. G. Souza · I. M. G. Santos (✉)
Laboratório de Combustíveis e Materiais/INCTMN, Departamento de Química, Universidade Federal da Paraíba, Campus I, João Pessoa, PB, Brazil
e-mail: ieda@quimica.ufpb.br

S. J. G. Lima
LSR, Departamento de Engenharia Mecânica/CT, Universidade Federal da Paraíba, Campus I, João Pessoa, PB, Brazil

E. Longo
LIEC/INCTMN, Instituto de Química, UNESP, Araraquara, SP, Brazil

Introduction

Perovskite structures have a simple crystalline structure, which includes different symmetries, as cubic, tetragonal or orthorhombic ones, besides distorted cells [1]. Because of their varied structure and composition, perovskite materials have attracted interest in many applied and fundamental areas of solid state chemistry, physics, advanced materials, and catalysis [2]. Alkaline earth stannates have recently become important materials in ceramic technology due to its use as humidity sensor [3]. The interest in $SrSnO_3$ compounds is related to its hability for Fe doping, formation of vacancies, besides oxidation or reduction of Fe^{3+} contribute to the stabilization of the perovskite phase [2, 4, 5]. This chemical behavior is reflected in the electronic structure of the solid compound band gaps characteristic of semiconductor [2].

According to Kim et al. [4] and Roh et al. [5], the difference in the oxidation state of Fe ions, Sn^{4+} and Sr^{2+} leads to an electroneutrality mismatch that is compensated by oxygen vacancies. When a higher amount of Fe ions replace Sn^{4+} in $SrSnO_3$, a higher amount of Fe^{3+} is oxidized to Fe^{4+}, leading to a lower amount of oxygen vacancies. This material has been previously synthesized using the solid state reaction, with a temperature treatment above 1000 °C/24 h [6].

In this work, Fe^{3+} doped strontium stannate ($SrSnO_3$) was synthesized by the polymeric precursor method. The polymeric precursor method, derived from the Pechini one, is characterized by the formation of a high amount of organic material favoring the formation of carbonates, especially when alkaline earth elements are present. As a consequence, the elimination of this organic material is an important factor which can change the short and long-range order [3]. The use of thermal analysis is very important in

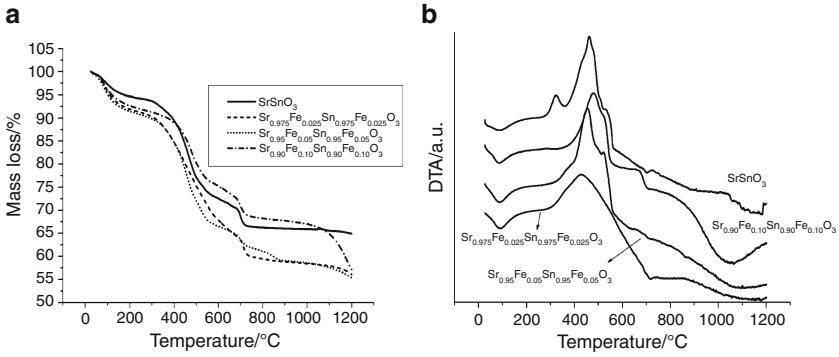

Fig. 1 **a** TG and **b** DTA curves of the powder precursors after heat treatment at 300 °C for 7 h in oxygen atmosphere

Table 1 Temperature and mass loss values determined by the TG curves of the precursors $SrSnO_3$ and $Sr_{1-x}Fe_xSn_{1-x}Fe_xO_3$ ($x = 0.025$, 0.05, and 0.10)

Sample	First step	Second step	Third step	Fourth step	Fifth step
$SrSnO_3$					
Temp range/°C	27–202	257–555	632–786	823–976	1016–1200
Mass loss /%	5.3	20.4	5.5	0.2	0.9
$x = 0.025$					
Temp range/°C	31–193	287–576	656–764	785–991	1010–1200
Mass loss/%	8.0	23.0	3.7	2.7	3.0
$x = 0.05$					
Temp range/°C	31–211	300–592	631–784	793–987	1003–1200
Mass loss/%	8.4	23.2	4.8	2.6	3.1
$x = 0.10$					
Temp range/°C	31–229	317–597	649–791	806–1005	1022–1200
Mass loss/%	7.6	15.6	5.5	1.2	9.3

the understanding of this process, in order to decrease the amount of carbonates in the final material, as they are difficult to eliminate after formation. Elimination of the organic material was evaluated by thermal analysis (TG/DTA) and infrared spectroscopy. X-ray diffraction was used to evaluate the crystallization, while UV–vis spectroscopy permitted to evaluate the Fe^{3+} transitions.

Experimental

In this work, $SrSnO_3$ and $Sr_{1-x}Fe_xSn_{1-x}Fe_xO_3$ ($x = 0.025$, 0.05, and 0.10) were synthesized by the polymeric precursor method using the methodology described in the literature [7]. The reagents used in the synthesis were: tin chloride di-hydrate (99.9%—J. T. Backer), strontium

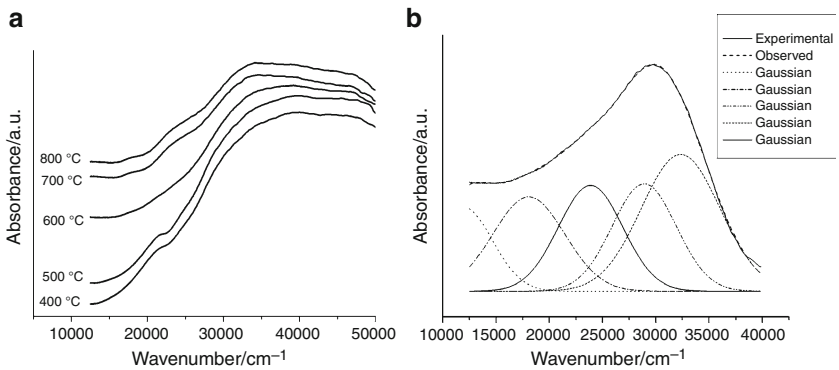

Fig. 2 **a** UV–vis spectra of for $Sr_{0.90}Fe_{0.10}Sn_{0.90}Fe_{0.10}O_3$ after calcination at different temperatures; **b** deconvolution of the UV–vis spectrum of the sample calcined at 600 °C, after spectral subtraction

Table 2 Spectral deconvolution results of the undoped $SrSnO_3$

Sample	400 °C	500 °C	600 °C	700 °C	800 °C	1100 °C	Assignment
Band (cm^{-1})	20,601	–	–	–	–	–	–
	28,852	–	–	–	–	–	–
	34,822	32,173	35,038	35,459	36,121	–	LMCT
	39,002	38,390	38,605	38,839	38,943	37,958	LMCT
	43,733	45,169	43,007	43,370	42,607	44,929	LMCT
	48,912	51,830	49,153	48,966	48,993	51,519	–

Table 3 Spectral deconvolution results of the $Sr_{0.90}Fe_{0.10}Sn_{0.90}Fe_{0.10}O_3$

Sample	400 °C	500 °C	600 °C	700 °C	800 °C	1100 °C	Assignment
Band (cm^{-1})	–	–	12,500	–	–	12,298	$^4T_{1g}$ (G)
	18,709	–	18,060	18,745	18,769	–	$^4T_{2g}$ (G)
	21,717	20,870	23,863	23,222	23,723	20,520	$^4A_{1g}$, ^4E_g
	29,214	29,023	28,910	27,875	29,000	26,696	$^4T_{2g}$ (D)
	32,876	32,040	32,240	32,659	33,278	32,624	$^4T_{1g}$ (P)

nitrate (99.0%—Vetec), iron nitrate nona-hydrate (P.A.—Vetec), ammonium hydroxide (P.A.—Vetec), nitric acid (65.0%—Dinâmica), citric acid (99.5%—Cargil), ethylene glycol (99.0—Avocado).

Carbon elimination was carried out by calcination of the precursor in O_2 atmosphere at 300 °C for 7 h, after milling of the precursors in an attritor mill for 4 h in alcoholic medium. The thermal characterization of the precursor was performed by thermogravimetry (TG) and differential thermal analysis (DTA), using a DTG-60 Shimadzu thermal analyzer. Samples of about 10 mg were heated at 10 °C min^{-1} up to 1200 °C in air atmosphere with a flow rate of 50 mL min^{-1}, inside alumina pans.

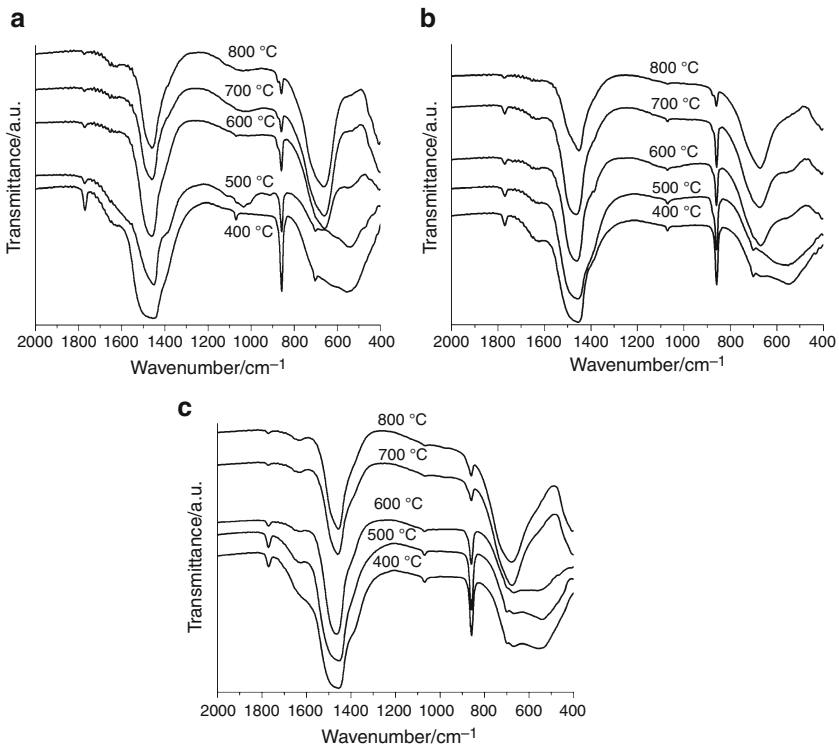

Fig. 3 IR spectra of the samples after heat treatment between 400 and 800 °C. **a** $SrSnO_3$; **b** $Sr_{0.90}Fe_{0.05}Sn_{0.90}Fe_{0.05}O_3$; **c** $Sr_{0.90}Fe_{0.10}Sn_{0.90}Fe_{0.10}O_3$

After thermal treatment at 400, 500, 600, 700, 800, and 1100 °C for 4 h, the material was characterized using X-ray diffraction (XRD), infrared spectroscopy (IR), and UV–visible spectroscopy (UV–vis). The XRD patterns were obtained using a D-5000 Siemens diffractometer, employing Cu (Kα) radiation, using continuous scanning mode in the 2θ range of 15°–85°, with a 0.02° step and a step time of 1.0 s. The IR analyses were performed using an IRPrestige-21 Shimadzu spectrophotometer, in the range from 4,000 to 400 cm^{-1}, using KBr pellets. UV–vis spectra were obtained, using an UV-2550 Shimadzu spectrophotometer, in the 190–900 nm range.

Results and discussion

Figure 1 shows the TG and DTA curves of the precursors and results are presented in Table 1. Five thermal decomposition steps were observed in the TG curves. In the first step, water and gases adsorbed on the powder surfaces were eliminated, with endothermic transitions in the DTA curves. The second step was assigned to the combustion of the organic material between 300 and 600 °C with exothermic peaks in the DTA curve. The mass losses associated to the endothermic peaks above 710 °C (third step) were assigned to the carbonate decomposition. In the present work the fourth step was assigned to the elimination of hydroxyls. Another mass loss was observed (fifth step) only for doped samples above 1000 °C, with the last endothermic peak at about 1080 °C for $Sr_{0.90}Fe_{0.10}Sn_{0.90}Fe_{0.10}O_3$. This mass loss may be assigned to Fe^{3+} reduction to Fe^{2+}, leading to the formation of oxygen vacancies or to decomposition of residual carbonates.

The UV–vis spectra were analyzed (Fig. 2; Tables 2, 3) in order to evaluate the iron oxidation state in doped perovskites. The sample $SrSnO_3$ exhibits an absorption band in the violet region, probably assigned to a ligand–metal charge transfer (LMCT) $O^{2-} \leftrightarrow Sn^{4+}$ analogue to the well-known $O^{2-} \leftrightarrow Ti^{4+}$ (LMCT) in rutile (Table 2) [8, 9].

Superposition among charge transfer and crystal field (CF) bands leads to difficulties in interpretation of the spectra. It was tried to overcome this drawback using the methodology proposed by Dondi et al. [8]. Elimination of the LMCT band was done by subtracting the contribution of the undoped $SrSnO_3$ from the visible spectrum and deconvolving the expected CF peaks (Fig. 2b; Table 3). Broad bands were obtained which were assigned to Fe^{3+} which belongs to d^5 configuration. When its electronic configuration has five unpaired electrons only spin-forbidden transitions from its ground state, $^6A_{1g}$ (S), occurs. Bands are expected at about 12,500–14,000 cm^{-1} $^6A_{1g} \rightarrow {}^4T_{1g}$ (^4G), 15,500–18,000 cm^{-1} $^6A_{1g} \rightarrow {}^4T_{2g}$

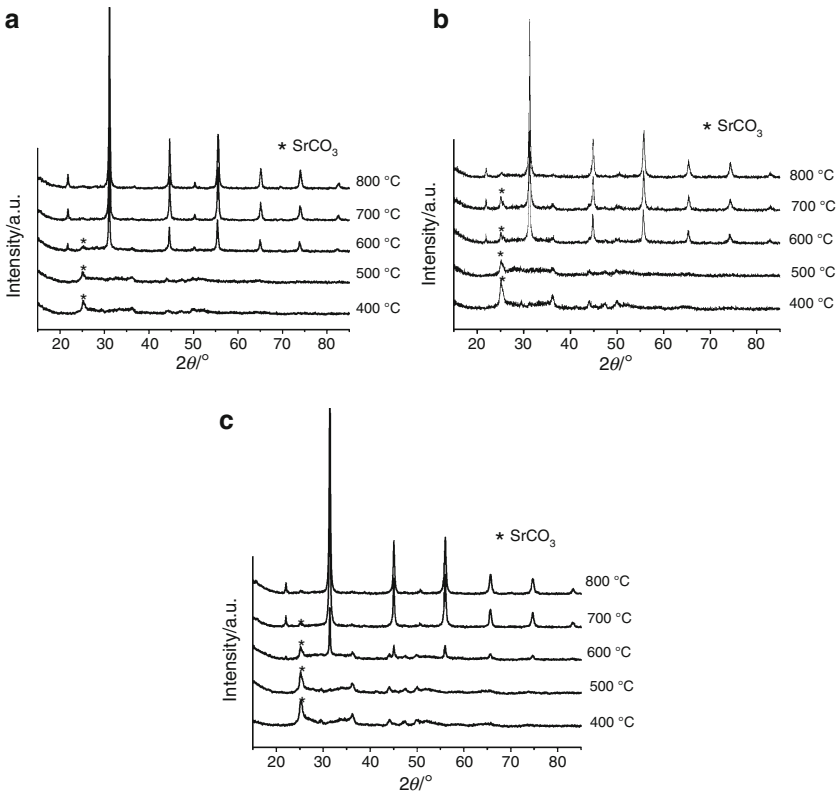

Fig. 4 XRD patterns of samples after heat treatment between 400 and 800 °C. **a** $SrSnO_3$; **b** $Sr_{0.90}Fe_{0.05}Sn_{0.90}Fe_{0.05}O_3$; **c** $Sr_{0.90}Fe_{0.10}Sn_{0.90}Fe_{0.10}O_3$

Table 4 Evaluation of the crystallinity according to the XRD patterns

Sample/°C	FWHM/°	Relative crystallinity/%
$SrSnO_3$		
600	0.20	13
700	0.22	37
800	0.23	50
$Sr_{0.90}Fe_{0.10}Sn_{0.90}Fe_{0.10}O_3$		
600	0.20	0
700	0.23	94
800	0.24	100

(^{4}G), 20,000–24,000 cm^{-1} $^6A_{1g} \rightarrow {}^4A_{1g}$ ^4E_g (G), 25,000–29,000 cm^{-1} $^6A_{1g} \rightarrow {}^4T_{2g}$ (^{4}D), and 30,000–33,000 cm^{-1} $^6A_{1g} \rightarrow {}^4T_{1g}$ (P) [10–12]. For the $Sr_{0.90}Fe_{0.10}Sn_{0.90}Fe_{0.10}O_3$ only absorption bands assigned to Fe^{3+} were observed, even after calcination at 1100 °C. These results indicated that mass loss above 1000 °C was not assigned to Fe^{3+} reduction.

The IR spectra of the powders are presented in Fig. 3. One band at 1630 cm^{-1} was observed indicating the presence of water. Bands at 1547 and 1389 cm^{-1} were assigned to chelated esters. The intensity of these bands decreased when heat treatment temperature increased. These results indicated that the exothermic peaks between 300 and 590 °C were due to the ester combustion. According to Nyquist and Kagel [13], carbonate bands are located at 1320–1530, 1040–1100, and 800–900 cm^{-1}, which were observed in all samples in the present work, but with lower intensities at higher temperatures, confirming the assignment of the third mass loss step to carbonate elimination.

According to Perry et al. [14], four vibration modes are present in perovskite infrared spectra: ν_1 is assigned to the stretch vibration of Me–O bond; ν_2 is an optically inactive mode of the stannate group (SnO_3^{2-}), which becomes active on account of distortions of the crystal lattice from ideal cubic structure; ν_3 is assigned to a stretching and bending mode of O–Sn–O; ν_4 is the only mode which depends on the modifier cation. In this work, ν_1 and ν_2 modes were observed at 670–540 and 400 cm^{-1}, respectively. With temperature increase, the intensity of the band at 540 cm^{-1} decreased while the intensity of the bands at 670 and 400 cm^{-1} increased. In the work published by Karlsson et al. [15], one band at 680 cm^{-1} appeared when a local structural distortion of the cubic structure occurred. In the present work, this distortion is related to the inclination among octahedra which is present when long-range order takes place, being characteristic of well crystallized stannate perovskites.

Iron doping made short range ordering more difficult. For $Sr_{0.90}Fe_{0.05}Sn_{0.90}Fe_{0.05}O_3$, the behavior at 600 °C was similar to the undoped sample but a higher intensity of the band at 540 cm^{-1} was observed at higher temperatures. For $Sr_{0.90}Fe_{0.10}Sn_{0.90}Fe_{0.10}O_3$ a high intensity of this band was observed even after calcination at 600 °C, decreasing at higher heat treatment temperatures.

XRD patterns (Fig. 4) showed the perovskite phase formation above 600 °C for all samples.

All diffraction peaks were indexed as orthorhombic perovskite according to the JCPDS file 77–1798 with space group *Pbnn*. Peaks assigned to $SrCO_3$ were also observed at low temperatures (starred peaks) with smaller intensities above 700 °C, confirming that the endothermic peak at 710 °C in DTA curve was due to carbonate decomposition as already showed by infrared spectra. SnO_2 precipitation was not observed.

In spite of the intensity decrease, carbonates were still observed after calcinations at 800 °C, as observed in infrared spectra and XRD patterns. These results indicated that the mass loss above 1000 °C was assigned to the elimination of residual carbonate.

A low crystallinity was observed for $Sr_{0.90}Fe_{0.10}Sn_{0.90}Fe_{0.10}O_3$ calcined at 600 °C, being smaller than the other samples heat treated at the same temperature. At 700 °C all samples showed a high crystallinity. Comparison to IR spectra indicated that short and long-range ordering occurred concomitantly. Comparing to literature data [1] iron doping did not make crystallization as difficult as neodymium did. For $SrSnO_3$:Nd, crystallization only started after calcination at 700 °C and SnO precipitation occurred indicating that Sn^{4+} reduction took place [1].

Long-range order was evaluate using the full width at half maximum (FWHM) for the (2 0 0) plane of the XRD patterns while the relative crystallinity was evaluate using the intensities of the same peaks (Table 4). Only a very small increase in the long-range disorder was observed with temperature. The relative crystallinity (%) had a different behavior with a higher crystallinity at higher temperatures. Fe^{3+} doping led to a higher crystallinity indicating that long-range order was attained in spite of the higher short range disorder showed in infrared spectra.

Conclusions

TG curves of the powder precursors indicated that the thermal decomposition process proceeded with four thermal decomposition steps. The first one was due to water and gases desorption. The exothermic peaks between 300 and 600 °C were due to the ester combustion. The third mass loss step was assigned to the carbonate decomposition as well as the last endothermic peak at about 1080 °C. The Fe^{3+} doping led to higher short range disorder but made

long-range crystallization easier. This behavior was related to the formation of defects in the structure.

Acknowledgements The authors acknowledge the project National Institutes of Science and Technology supported by the National Council for Scientific and Technological Development (INCT/CNPq/MCT), Research and Projects Financing (FINEP/MCT), and Petrobras for the financial support.

References

1. Souza SC, Alves MCF, Oliveira ALM, Longo E, Vieira FTG, Gomes RM, Soledade LEB, Souza AG, Santos IMG. $SrSnO_3$:Nd obtained by the polymeric precursor method. J Therm Anal Calorim. 2009;97:85–190.
2. Tejuca LG, Fierro LG. Properties and applications of perovskite-type oxides. New York: Marcel Pekker INC; 1993.
3. Alves MCF, Souza SC, Silva MRS, Paris EC, Lima SJG, Gomes RM, Longo E, Souza AG, Santos IMG. Thermal analysis applied in the crystallization study of $SrSnO_3$. J Therm Anal Calorim. 2009;97:179–83.
4. Kim MG, Cho HS, Yo CH. Fe K-edg X-ray absorption (XANES/EXAFS) spectroscopic study of the nonstoichiometric $SrFe_{1-x}Sn_xO_{3-x}$ system. J Phys Chem Solids. 1998;59:1369–81.
5. Roh KS, Ryu KH, Yo CH. Nonstoichiometric and physical properties of the $SrSn_{1-x}Fe_xO_{3-x}$ system. J Solid State Chem. 1999;142:288–93.
6. Beurmann PS, Thangadurai V, Weppner W. Phase transitions in the $SrSnO_3$–$SrSnO_3$ solid solutions: X-ray diffraction and Mössbauer studies. J Solid State Chem. 2003;174:392–402.
7. Alves MCF, Souza SC, Lima SJG, Longo E, Souza AG, Santos IMG. Influence of the precursor salts in the synthesis of $CaSnO_3$ by the polymeric precursor method. J Therm Anal Calorim. 2007;87:763–6.
8. Dondi M, Cruciani G, Guarini G, Matteuci F, Raimondo M. The role of counterions (Mo, Nb, Sb, W) in Cr, Mn, Ni and V doped rutile ceramic pigments Part 2. Colour and technological properties. Ceram Int. 2006;32:393–405.
9. Dondi M, Matteucci F, Cruciani G. Zirconium titanate ceramic pigments: crystal structure, optical spectroscopy and technological properties. J Solid State Chem. 2006;179:233–46.
10. Rao JL, Murali A, Rao ED. Electron paramagnetic resonance and optical spectra of Fe(III) ions in alkali zinc borosulphate glasses. J Non Cryst Solids. 1996;202:215–21.
11. Reddy KN, Reddy GS, Reddy SL, Roo PS. Optical absorption and EPR spectral studies of vauquelinite. Cryst Res Technnol. 2006;41:818–21.
12. Taran NM, Langer K. Electronic absorption spectra of Fe^{3+} in andradite and epidote at different temperatures and pressures. Eur J Mineral. 2000;12:7–15.
13. Nyquist R, Kagel R. Infrared spectra of inorganic compounds. London: Academic Press; 1971.
14. Perry CH, Mccarthy DJ, Rupprecht G. Dieletric dispersion of some perovskite zirconates. Phys Rev. 1965;138:1537–8.
15. Karlsson M, Matic A, Knee CS, Ahmed I, Eriksson SG, Borjesson L. Short-Range structure of proton-conducting perovskite $BaIn_xZr_{1-x}O_{3-x/2}$ (x = 0–0.75). Chem Mater. 2008;20:3480–6.